Swiss Journal of Palaeontology (2026) 145: 881–900 | DOI 10.3897/sjp.145.193019

PENSOFT

Swiss Journal of Palaeontology

SGG SGS

scnat swiss academy of sciences

Research Article

Lizards under pressure: skull nanoindentation in an insular reptile for palaeobiological inference

Laia Garcia-Escolà[1], Jordi Marcé-Nogué[2], Ane de Celis[1,3], Núria Cuadrado[4,5,6], Eduard Vidales[4], Penélope Cruzado-Caballero[7,8], Alejandro Serrano-Martínez[1], Carolina Castillo-Ruiz[7], Josep Fortuny[1]

1 *Institut Català de Paleontologia Miquel Crusafont (ICP-CERCA), Universitat Autònoma de Barcelona, Edifici ICTA-ICP, c/ de les Columnes s/n, Campus de la UAB, 08193 Cerdanyola del Vallès, Barcelona, Catalonia, Spain*

2 *Universitat Rovira i Virgili, Department d'Enginyeria Mecànica, Campus Sescelades, Edifici E4, Avinguda Països Catalans 26, 43007 Tarragona, Spain*

3 *Grupo de Biología Evolutiva, Facultad de Ciencias, Universidad Nacional de Educación a Distancia, Avenida Esparta s/n, Las Rozas de Madrid, 28232, Madrid, Spain*

4 *Eurecat, Centre Tecnològic de Catalunya, Unit of Metallic and Ceramic Materials, Plaça de la Ciència 2, 08243, Manresa, Spain*

5 *Universitat Politècnica de Catalunya, Department of Science and Material Engineering Av. Eduard Maristany, 10-14, 08019, Barcelona, Spain*

6 *Universitat de Vic – Universitat Central de Catalunya, MECAMAT, Facultat de Ciències i Enginyeries, C. De la Laura, 13, 08500 Vic, Spain*

7 *Universidad de La Laguna, Departamento de Biología Animal, Edafología y Geología, Av. Astrofísico Francisco Sánchez s/n, San Cristobal de La Laguna, 38200, Spain*

8 *Universidad de Zaragoza, Facultad de Ciencias, Aragosaurus: Recursos Geológicos y Paleoambientes-IUCA 50009, Zaragoza, Spain*

https://zoobank.org/DD442AD1-4F4E-4B30-8EDF-4DDA24ACDC14

Corresponding authors: Laia Garcia-Escolà (laia.garcia@icp.cat); Josep Fortuny (josep.fortuny@icp.cat)

Academic editor: Rémi Lefebvre ♦ **Received** 30 March 2026 ♦ **Accepted** 24 July 2026 ♦ **Published** 19 August 2026

Abstract

Computational approaches are increasingly used to study the relationship between form and function in extinct and living organisms. However, one major challenge remains: assumptions about bone material properties, especially when studying fossils. In this work, direct mechanical testing and computer-based modelling are combined to assess cranial bone stiffness in the lizard genus *Gallotia*, endemic to the Canary Islands (Spain), including extinct species. Using linear mixed models, bone stiffness was found to be uniform across skull regions, with a trend towards lower stiffness in larger species. Simulations of biting loads showed that differences in bone properties had a limited influence on mechanical performance, supporting the use of average values in functional models. Using this framework, bone stiffness in extinct *Gallotia* giants was estimated, and its significance was explored. The results suggest a link between skull flexibility, body size, and diet, offering a practical approach to reconstructing biomechanical traits in extinct vertebrates across evolutionary timescales.

Keywords

Bone mechanical properties, finite element analysis, *Gallotia*, inference, insular, nanoindentation, Young's modulus

Introduction

In recent years, there have been notable advancements in the field of computational biomechanics, with finite element analysis (FEA) becoming a prevalent tool in zoological and palaeontological research to examine the form and function of biological structures (Rayfield 2007; Krings et al. 2021; Della Giustina 2026). This method allows researchers to model stress, strain, and deformation in complex biological structures, significantly

contributing to our understanding of biomechanics and functional morphology in both living and extinct organisms, especially vertebrates (Rayfield 2007; Garcia-Escolà et al. 2024; Mitchell et al. 2025).

However, the reliability of such biomechanical analyses in extinct species depends heavily on the availability of precise material properties for bony structures and soft tissues, which are rarely preserved in the fossil record. To overcome this limitation, palaeobiologists often employ the extant phylogenetic bracket (EPB) (Witmer 1995) or seek ecological analogues with available material data (e.g. McGuire and Dudley 2011; Cuff and Rayfield 2013). These approaches, however, inherently present several challenges. In particular, the available data are very limited across many vertebrate groups – particularly reptiles (Currey 1987; Erickson et al. 2002; Cuff et al. 2015; Jones et al. 2017; Dutel et al. 2021; Marghoub et al. 2022; Suppl. material 9: table S1) – and are subject to several factors, such as ontogeny or sex, which may significantly affect the results (Brown and Vavrek 2015).

In finite element models of extinct taxa, it is common to assign material properties derived from extant species, including mammalian cortical bone (often from bovine samples), avian bone, or extant crocodylian bone (Mazzetta et al. 2009; Aguirre et al. 2020), to model dinosaur skulls or other reptilian structures (Button et al. 2014). While this approach facilitates model construction, it may introduce substantial inaccuracies because the mechanical properties of these analogues can differ considerably from those of the extinct taxa they are intended to represent. These limitations highlight the importance of obtaining direct mechanical data from extant vertebrates to improve the accuracy of biomechanical models.

An ideal system for addressing these questions is provided by the endemic Canary Island genus *Gallotia* (Squamata: Lacertidae), which exhibits substantial interspecific variation in body size (ranging from <70 mm SVL in *G. atlantica* to >500 mm in *G. goliath*; Mateo et al. 2022), ecology, and diet, making it particularly suitable for studying how variation in bone material properties may influence cranial biomechanics and functional adaptation.

To explore these relationships, the skull represents a particularly informative structure. The vertebrate skull reflects a trade-off between multiple functional demands, often involving conflicting roles. These include protecting the brain and sensory structures from external forces and efficiently processing food through biting and prey manipulation (e.g. Lautenschlager et al. 2018; Paluh and Bauer 2018).

In lizards, biting, prey resistance, and the associated muscle activities subject the skull to considerable mechanical loads that must be absorbed to prevent damage to the brain and sensory organs (Evans 2008). The relatively lightweight lepidosaur skull must therefore balance its protective and active functions, allowing for strong bite forces without compromising structural integrity. In squamates, including the lizard genus *Gallotia*, the loss of the lower temporal bar – retained in the rhynchocephalian lepidosaur *Sphenodon* – resulted in the decoupling of the anterior and posterior skull regions, increasing cranial kinesis (Evans 2008). The absence of contact between the jugal and the quadrate enables the latter to pivot around its dorsal end, a movement known as streptostyly. Detailed descriptions of lepidosaur cranial anatomy and osteology are provided by Evans (2008) and Villa and Delfino (2019), whereas anatomical studies specifically focused on *Gallotia* can be found in Barahona et al. (1998), Cruzado-Caballero et al. (2019), Palacios-García et al. (2021) and Pérez-Martín et al. (2023).

Lizard skulls also reflect an evolutionary trend towards the reduction of cranial elements, tending to be lighter than those of their ancestors. This reduction in skeletal mass is associated with a decrease in the relative mass of the jaw adductor muscles, with functional implications for bite force and feeding behaviour (Herrel et al. 2014). Moreover, the repeated and independent reduction or loss of the postorbital bar in squamates is linked to remarkable diversity in cranial architecture, making their skulls an ideal system for investigating functional trade-offs and structural constraints (Barel 1983).

An increase in bite force usually parallels an enlargement of the jaw adductor muscles and a more solid cranial structure (Herrel et al. 1999; Moazen et al. 2008). Nevertheless, a stronger bite often comes at the expense of speed because lever geometry and muscle contraction dynamics impose mechanical limits on both functions. Consequently, species that rely on capturing agile or fast-moving prey typically develop longer, more slender snouts, favouring rapid jaw closure over forceful biting (Herrel et al. 2001; Westneat 2003). In some lizards, an additional form of cranial kinesis – mesokinesis, i.e. bending of the skull at the frontoparietal region – can also occur, rendering some skulls dikinetic (i.e. exhibiting movement at two cranial joints) (Montuelle and Williams 2015). However, phylogenetic analyses (Mezzalira 2013) and histological studies (Iordansky 2010) provide no clear evidence for meso- or metakinesis in lacertids, the family to which *Gallotia* belongs. Unlike other lepidosaur groups, such as gekkotans or varanids, lacertids do not show kinesis at the frontoparietal junction, which tends to become more rigid in adults (Barahona et al. 1998).

In this context, nanoindentation was applied to several *Gallotia* species (*G. atlantica*, *G. stehlini*, and *G. galloti*) selected for their variation in body size and feeding ecology, providing a comparative framework for investigating cranial bone properties.

Nanoindentation is a high-resolution technique that measures mechanical properties, such as Young's modulus (E), across submicrometric and microstructural scales, providing key information for multiple applications, such as computational biomechanical analysis. Its applications in biomedical and biological materials research are well established, providing insights into biological structures such as bone, tooth enamel, seeds, insect cuticles, and fish scales (Cuy et al. 2002; Allison

et al. 2014). In vertebrates in general, however, studies applying nanoindentation remain very scarce and are even rarer in reptiles (see Suppl. material 9: table S1). Moreover, most available studies rely on a single measurement point for entire structures, such as the skull, which can overlook the inherent spatial variability of material properties. Obtaining localised data across multiple regions of the same skull is especially valuable, as it captures the natural heterogeneity of cranial bone rather than relying on averaged values (Rodríguez-Florez et al. 2013; Wang et al. 2024).

Here, nanoindentation measurements across several *Gallotia* species with differing ecological adaptations provide critical information to improve the biological realism of FE models while also allowing inferences about how cranial bone material may have evolved in response to environmental pressures. The selected species (*G. atlantica*, *G. stehlini*, and *G. galloti*) represent a broad range of body sizes and feeding behaviours within the genus, providing a comparative framework for investigating cranial bone mechanical properties.

The main objective is to address the current scarcity of data on the physical and biomechanical properties of lizard skulls and jaws, using *Gallotia* as a paradigmatic case study. Importantly, some *Gallotia* species are critically endangered (e.g. *G. simonyi*, *G. bravoana*, *G. stehlini*, and *G. intermedia*), while others (e.g. *G. auaritae* and *G. goliath*) have become extinct in recent times. This highlights the importance of integrating data from both extant and fossil taxa to better understand evolutionary patterns, functional adaptations, and extinction processes through time, providing a broader framework for interpreting the ecological and biomechanical diversification of insular species and their conservation significance. Two alternative hypotheses were tested to evaluate the influence of bone material heterogeneity on FEA outcomes:

A. The heterogeneous hypothesis: realistic and biologically meaningful results require incorporating spatial variation in bone stiffness across the skull.
B. The homogeneous hypothesis: the mechanical response of the skull can be adequately represented using a uniform Young's modulus value averaged across all sampled regions. This approach assumes that local differences in material stiffness do not significantly affect global stress or strain patterns in the model.

Furthermore, as the genus includes both extant and extinct species, this study pioneers the estimation of the mechanical properties of extinct giant species, such as *Gallotia goliath*. These findings not only contribute to the advancement of current biomechanical modelling but also establish a framework for future palaeobiological research, enhancing our understanding of evolutionary adaptations in prehistoric vertebrates and providing new clues on conservation (palaeo)biology for endangered extant species.

Materials and methods

Nanoindentation

Five specimens representing three different extant *Gallotia* species were analysed (Table 1), including individuals from giant and non-giant species within the genus, with ontogenetic variation present in *G. stehlini*.

All five specimens were recovered already dead in the field as a consequence of bird predation (shrikes for *G. atlantica* and juvenile *G. stehlini* specimens and kestrels for the *G. galloti* specimen), except for the adult *G. stehlini* specimen, which was provided already dead by the Tafira Wildlife Rehabilitation Centre (Gran Canaria Island, Spain), with an unknown cause of death. The *G. atlantica* and juvenile *G. stehlini* specimens were exposed before collection (post-mortem interval) for a maximum of 2 weeks, since regular culls were carried out. For the *G. galloti* specimen, the post-mortem interval was approximately 3–4 days, while for the adult *G. stehlini* specimen, collection occurred a few hours after death. The sex of the specimens is unknown.

Once recovered, all the specimens were immersed in water for 1 h to facilitate the extraction of skin and soft tissue. These individuals were subsequently used exclusively for nanoindentation analyses, with material sampling carried out independently from the specimens used in biomechanical modelling to preserve their integrity.

Due to the complex geometry of the skull and the need to access specific anatomical regions, each skull was fully embedded in a transparent cold-curing epoxy resin (Struers Epofix Resin). This avoided exposure to heat or pressure and ensured the production of a planoparallel block. The embedding process required approximately 8 h for complete curing of the resin.

Skull samples from the different species were fully embedded, and the targeted regions were accessed through

Table 1. List of specimens analysed using the nanoindentation method.

Taxon	Label	Location	Life stage	Skull length [mm]
G. atlantica	020322-4	El Islote (San Bartolomé, Lanzarote)	Adult	18.56
G. galloti	G.galloti/21-1	Sciences Faculty – Universidad de La Laguna (Tenerife)	Adult	29.52
G. stehlini	040322-1	Playa de Vargas, Agüimes (Gran Canaria)	Juvenile	27.40
	040322-3	Playa de Vargas, Agüimes (Gran Canaria)	Juvenile	21.66
	GAST492-22	Centro de Recuperación de Fauna Silvestre de Tafira (Gran Canaria)	Adult	61.10

sequential polishing. Polishing was performed starting from the upper surface of the skull, progressively exposing the areas of interest for analysis. Polishing was conducted using Struers abrasive paper with a grit size of P240 until the region of interest was exposed. Subsequently, standard polishing was performed with 1200-grit SiC paper, followed by fine polishing using diamond suspensions of 3 µm and 1 µm. Finally, an OP-S colloidal silica suspension with a particle size of 40 nm was applied to obtain a mirror-like finish. Although surface roughness was not quantitatively measured, polishing was continued until the desired surface appearance was achieved, ensuring that any residual surface irregularities did not compromise the reliability of the nanoindentation results (Suppl. material 9: fig. S1).

To investigate material properties, extant specimens were analysed using nanoindentation to assess the evolution of the contact response during loading and unloading, from which Young's modulus (*E*) was obtained following the Oliver–Pharr method (Oliver and Pharr 1992; Oliver and Pharr 2004), providing an indication of the elastic response of the material. The nanoindenter, equipped with a Berkovich pyramidal tip, was used to obtain several measurements across each selected region of interest. Nanoindentation arrays were subsequently performed on 11 areas of interest across the cranium and mandible, as described in Table 2, including seven regions of bone (B1–B7), two cranial sutures (S8, S9), and two tooth-related areas (D10, dentine, and E11, enamel). Tests were performed under load-controlled conditions, with the maximum load set to 2 mN. A high-speed indentation system capable of generating material property maps was used. Nanoindentation mappings were performed using a Berkovich tip at a test frequency (load–hold–unload) of 100 kHz. At the specified load, the indentation depth and contact stiffness were recorded, enabling the calculation of Young's modulus using the Oliver–Pharr method (Oliver and Pharr 1992; Oliver and Pharr 2004).

Table 2. Locations and material types analysed using the nanoindentation method.

ID	Area of interest	Material
B1	Anterior region of the premaxilla	Bone
B2	Central part of the parietal	Bone
B3	Quadrate (Adjacent to the suture)	Bone
B4	Central region of the pterygoid	Bone
B5	Central region of the orbital osteoderm	Bone
B6	Middle-upper region of the coronoid	Bone
B7	Inner central part of the dentary	Bone
S8	Triple sutural contact area of frontals and parietal	Suture
S9	Vomer-palatine suture	Suture
D10	Cranium caudal tooth	Dentine
E11	Cranium caudal tooth	Enamel

Given the size of the regions analysed, the spacing between indentations within each array was set to 8 µm. This ensured complete coverage of the area while preventing interaction between the stress fields generated by adjacent indentations. Considering the Berkovich tip geometry used in the tests, the relationship between penetration depth and indentation size was evaluated to confirm that the selected spacing avoided mutual influence between neighbouring indents, thereby ensuring the reliability of the measurements. Achieving the 8 µm spacing required an applied load of 2 mN. In each area of interest, the dimensions of the arrays were adjusted to the specimen size (see Suppl. material 1), and the average *E* values were derived from the resulting maps (Suppl. materials 2–6). A Shapiro–Wilk test was conducted on the *E* measurements, rejecting the assumption of normality ($p < 0.05$). Consequently, median *E* values and mean absolute deviation (MAD) were computed for each location to provide a robust representation of both central tendency and variability (Figs 2, 3, Suppl. material 9: fig. S3; Table 4).

Nanoindentation analyses were conducted under a legal permit issued by the Canary Government (Exp. 33-2023-0524072603).

Statistical analyses and linear mixed models (LMMs)

Young's modulus of the cranial bone areas of interest (*E*) was analysed to test whether there were differences in *E* among the seven cranial areas (B1–B7) and to assess whether dorsal cranial length (DCL) was a reliable predictor of *E* for extrapolation to fossil specimens of the same genus, *Gallotia*. Because *E* measurements constitute pseudoreplicates (multiple measurements per cranial area) nested within cranial areas and specimens, linear mixed-effects models (LMMs) were applied to account for the hierarchical, non-independent structure of the data.

Prior to conducting the LMMs, outliers for each cranial area and specimen were identified visually using Q–Q plots and boxplots generated with ggplot2 v4.0.0 in R (Wickham 2016; R Core Team 2018) and quantitatively using Tukey's 1.5 × IQR method (Tukey 1977; Hoaglin et al. 1986). Descriptive statistics were calculated with psych v2.5.6 in R (Revelle 2025) on datasets both including and excluding these outliers to ensure that the removal of these atypical values would not negatively affect the analyses. The 95% confidence intervals (CIs) for the mean *E* value of each extant specimen were calculated from the observed data using standard *t*-based intervals (the dataset is available in Suppl. material 7, and the full scripts for descriptive statistics and LMMs are available as Suppl. material 8).

First, to test for differences in *E* among cranial areas (B1–B7), only adult individuals ($n = 3$) were included in the LMM (LMM 1) to ensure a balanced design and to allow the fixed effect to be estimated independently. In this model, "*E*" was the dependent variable, and "Cranial Area" was included as a fixed effect, whereas the random effect "1|Specimen:CranialArea" accounted for the non-independence and clustering of repeated

measurements, resulting in the following model structure: $E \sim$ CranialArea + (1|Specimen:CranialArea).

To study the relationship between *E* and DCL, an additional LMM (LMM 2) was fitted, including DCL, Cranial Area, and Ontogeny as fixed effects and Specimen as a random effect, resulting in the model structure "$E \sim$ DCL + CranialArea + Ontogeny + (1|Specimen:CranialArea)". This second LMM included juveniles of *G. stehlini* (n = 2) alongside all adults to introduce sufficient variation in DCL, allowing estimation of its fixed effect on *E* while controlling for ontogeny, adjusting for any variation in *E* among cranial areas, and accounting for specimen-level random variability and nested repeated measurements of *E*.

The inclusion of juveniles increased the overall variability in DCL between specimens, since cranial length varies across species in adults and across ontogenetic stages in *G. stehlini* in this dataset. This greater between-specimen variation improves the estimation of the fixed effect of DCL and helps mitigate potential collinearity with other predictors. However, due to sample limitations, the fixed effect Ontogeny is partially confounded with Specimens/Species; therefore, the ontogenetic effect in this model must be interpreted with caution, as it may also reflect interspecific or specimen-specific differences rather than true developmental effects, a common challenge in studies of ontogenetic allometry when sample sizes and ontogenetic data are limited (Klingenberg 1998; Brown and Vavrek 2015). Because of the limited sample size and the purpose of the LMM, interaction terms between fixed effects (e.g. Cranial Area × Ontogeny) were not included in this LMM to avoid overparameterisation.

Model assumptions were verified by inspecting the residuals of the LMMs, and model diagnostics were performed using the R packages lme4 v1.1-37 (Bates et al. 2015) and performance v0.15.2 (Lüdecke et al. 2021). Normality was assessed using Q–Q plots and histograms of residuals, whereas homoscedasticity was evaluated by plotting the residuals against fitted values. Variance components for random effects indicated meaningful variation among specimens and cranial areas; therefore, the random effects in both LMMs correctly captured the nested structure of the data and pseudoreplicates. Collinearity among the fixed effects was inspected in LMM 2, which included three fixed effects, and the results of the variance inflation factors (VIFs) indicated low collinearity (VIF < 1.2). Since no substantial deviations from model assumptions were detected, no data transformations or additional procedures were required to fit the models. Both LMMs were adjusted using restricted maximum likelihood (REML) with the lme4 v1.1-37 package in R. To evaluate the significance of fixed effects in each LMM, type III ANOVAs with Satterthwaite approximation for degrees of freedom were performed using the lmerTest v3.1-3 package in R (Kuznetsova et al. 2017). In LMM 1, this ANOVA tested for differences in *E* among cranial areas, accounting for the random effect "Specimen:CranialArea", while in LMM 2, it assessed the relationship between *E* and DCL while accounting for Cranial Area and Ontogeny as fixed effects and the random effect "Specimen:CranialArea".

Young's modulus (E) extrapolation on fossil Gallotia specimens

To estimate Young's modulus (*E*) of fossil *Gallotia* specimens, the second LMM (LMM 2) fitted to the extant *Gallotia* dataset was used to predict *E* values for each cranial area based on the fossil's DCL and ontogenetic stage (adults). Predictions were obtained using only the fixed effects of LMM 2, thereby obtaining *E* values representing a typical *Gallotia* specimen with ggeffects v2.3.1 (Lüdecke 2018) and the stats v4.5.1 base package in R. This procedure allowed the extrapolation of *E* values for extinct *Gallotia* taxa (*G. goliath* and *G. auaritae*) from the allometric relationship observed between DCL and *E* in extant *Gallotia* specimens. The 95% CIs for extrapolated *E* values in fossils were estimated via parametric bootstrap (1,000 iterations) using the bootMer function from the lme4 v1.1-37 package in R. In each bootstrap iteration, model parameters were resampled from their estimated distribution, and *E* values were subsequently predicted for each cranial area and averaged to obtain a mean cranial *E* value for each fossil specimen. The 95% CIs were calculated for both individual cranial areas and mean cranial *E* values as the 2.5th and 97.5th percentiles of the corresponding bootstrap distributions.

Finite element analysis

Finite element analysis (FEA) was conducted to evaluate biomechanical performance during biting, with a primary focus on comparing the effects of different mechanical properties of the bone. Models were generated for three extant *Gallotia* species and one extinct species (*G. goliath*), resulting in a total of seven models: four models using homogeneous material properties and three other models using heterogeneous properties, except for *G. goliath*, for which only homogeneous properties could be assigned due to the lack of region-specific material property data. The models were designed to include muscular forces as intrinsic scenarios, which enabled the generation of biting models of the lizards.

Specimens were micro-CT scanned at the Centro Nacional de Investigación sobre la Evolución Humana (CENIEH, Burgos, Spain) using a GE Phoenix V|Tome|Xs240 mCT scanner (see Table 3 for specimen and scanning details). Scanning parameters were adjusted to maximise the resolution of the CT images according to specimen size. In particular, the fossil specimen *G. goliath* DZUL24553 required different scanning settings due to its large size and fossil preservation compared with the extant specimens. Raw data were processed in Avizo v.2023 (Thermo Fisher Scientific) to segment and generate

Table 3. Micro-CT-scanned specimens and technical information. The *G. goliath* specimen was originally published by Castillo et al. (1994).

Species	Label	Life stage	Voltage (kV)	Current (mA)	Voxel size (mm)	Mesh size (elements)	Mesh size (nodes)
G. atlantica	TFMC-VR-119	Adult	125	100	0.01500003	10928026	2082160
G. galloti	TFMC-VR-115	adult	130	170	0.02499963	12154884	2262706
G. stehlini	TFMC-VT-96	adult	130	170	0.0397195	7763489	1458323
G. goliath	DZUL2453	adult	150	250	0.11400021	1474134	2272278

3D surfaces. After segmentation, a CAD model of each specimen was created using Geomagic Wrap. During this last step, surface irregularities were repaired using refinement and smoothing tools, and the models were imported into ANSYS 2024 R1 software to perform FEA (Marcé-Nogué et al. 2011). See Suppl. material 9: text S1 for additional information. A static structural analysis was performed on the skulls of the four different *Gallotia* specimens using the finite element package ANSYS 2024 R1 on an HP Z6 G4 Workstation with 96 GB (8 cores × 12 GB) and 1.90 GHz. All the models were meshed with an adaptive mesh of tetrahedral elements (Marcé-Nogué et al. 2011) to appropriately capture the distribution patterns of stress and strain. Depending on the model, the meshes contained between 1.5 and 2.5 million nodes (Table 3).

Mechanical response was assessed using von Mises stress and principal strains (maximum and minimum). Von Mises stress was selected as an adequate criterion for predicting the yield of ductile materials when isotropic material properties are used in cortical bone (Doblaré et al. 2004). Principal strains, on the other hand, were used to evaluate the deformation response of the skull under mechanical loads resulting from differences in material stiffness. Therefore, they serve as a good indicator for assessing the influence of heterogeneity and homogeneity in the distribution of *E* (Keyak et al. 1998; Cowin 2001; Gómez-Benito et al. 2005).

Elastic and linear material properties were assumed for the bone. As mentioned above, two different approaches were used in all the models to compare the differences between a homogeneous material and a heterogeneous material. In the first approach, homogeneous properties were assumed for the bone using the following values for a reptile skull: *E* as the average value of all the bony locations (Table 4) and Poisson's ratio $\nu = 0.3$. The second approach used the different values from the nanoindentations to recreate a heterogeneous material (Table 4). The *E* values were assigned to the same points of the models where they were analysed. Using the thermal diffusion method implemented in ANSYS, the experimentally measured *E* values were interpolated across the skull to generate a continuous spatial distribution of material properties (Krings et al. 2021). In this context, the thermal field was not used to represent heat transfer but rather as a numerical proxy to smoothly diffuse the elastic values between adjacent elements, minimising abrupt transitions that could cause artificial stress concentrations. This approach allows a more realistic representation of the gradual variation in bone stiffness across cranial regions. Sutures, dentine, and enamel were excluded from the diffusion process to facilitate comparison with the homogeneous models and to specifically assess the influence of interspecific differences in bone material properties.

A simple loading scenario was analysed, considering an intrinsic case of bilateral biting on both the left and right sides of the skull in the rostral position. To simulate biting, fixed vertical displacements at the tooth positions were included to replicate prey capture. Movements of the skull were restricted using joints that allow rotation but not displacement, simulating, first, the jaw-joint contact and, second, the condyle and the presence of the vertebral column (Fig. 1).

Muscle forces were estimated using the standard biomechanical relation $F = \sigma \times PCSA$, where PCSA (physiological cross-sectional area) represents the area perpendicular to the muscle fibres and correlates with the maximum isometric force a muscle can produce. PCSA was used instead of the anatomical cross-sectional area (ACSA), as it better reflects the muscle's force-generating potential. Because detailed architectural parameters (fibre length and pennation angle) were unavailable, PCSA was approximated as the mean value between the cranial (origin) and mandibular (insertion) attachment areas for each muscle, a simplification commonly applied in comparative and palaeobiomechanical modelling (Alexander 1992).

Moreover, a uniform specific tension of $\sigma = 0.3$ MPa was assigned to all muscles, following McNeill Alexander (1992). This value is widely adopted in vertebrate biomechanics as a representative estimate of maximal contraction pressure, and it provides a consistent basis for comparing muscle forces across taxa. Although some variation may occur among species or developmental stages, specific tension is generally considered a conservative property of skeletal muscle, and using a uniform value helps to minimise additional assumptions about species-specific physiology.

Muscle forces were applied as distributed loads over their attachment areas, with directions defined by vectors connecting the centroids of each muscle's origin and insertion sites. Ten major jaw adductor muscles were included, representing the principal contributors to biting performance in lizards (see Suppl. material 9: tables S2–S5).

Institutional abbreviations: DZULL, Department of Zoology, Universidad de La Laguna (Tenerife, Canary Islands, Spain); PCCRULL, Palaeontology Collection – Carolina Castillo Ruiz, Universidad de La Laguna (Tenerife, Canary Islands, Spain).

Table 4. Median Young's modulus (GPa) and mean absolute deviation (MAD) for each region of interest across the five specimens analysed using the nanoindentation technique. Values were rounded to the nearest whole number. Note that data from locations B4 and E11 were not available for the specimen *G. stehlini* (040322-3). The average value considers the bone areas of interest as a whole for each analysed specimen.

Taxon	Label	B1	B2	B3	B4	B5	B6	B7
G. atlantica	020322-4	23.21 ± 2.31	22.43 ± 2.83	19.65 ± 1.58	19.68 ± 2.86	18.72 ± 2.67	25.32 ± 1.75	28.46 ± 1.87
G. galloti	G.galloti/21-1	17.66 ± 2.00	17.17 ± 2.78	25.14 ± 2.37	22.68 ± 2.61	19.71 ± 2.66	18.52 ± 1.65	25.87 ± 4.77
G. stehlini	GAST492-22	13.87 ± 1.30	20.57 ± 2.42	18.58 ± 1.78	22.47 ± 4.02	16.56 ± 2.60	13.97 ± 2.77	15.88 ± 1.46
G. stehlini	040322-1	15.55 ± 1.62	17.16 ± 4.07	14.94 ± 1.55	19.69 ± 2.13	16.57 ± 2.68	17.58 ± 1.39	21.26 ± 2.26
G. stehlini	040322-3	17.41 ± 1.28	23.38 ± 2.61	20.38 ± 5.02	NA	20.04 ± 2.65	14.36 ± 2.31	24.61 ± 2.42
		S8	**S9**	**D10**	**E11**	**Median E per specimen (BONE) ± MAD**		
G. atlantica	020322-4	4.56 ± 1.44	5.90 ± 1.82	20.82 ± 1.66	63.96 ± 3.27	24.31 ± 4.08		
G. galloti	G.galloti/21-1	4.06 ± 0.35	7.84 ± 1.89	19.76 ± 1.55	68.04 ± 8.39	18.97 ± 3.05		
G. stehlini	GAST492-22	5.02 ± 1.56	7.71 ± 1.81	14.74 ± 1.44	68.38 ± 7.58	16.96 ± 3.21		
G. stehlini	040322-1	4.47 ± 1.05	4.76 ± 0.98	19.22 ± 1.56	82.20 ± 8.85	17.19 ± 2.91		
G. stehlini	040322-3	4.61 ± 1.60	2.69 ± 1.55	18.18 ± 1.39	NA	16.88 ± 3.85		

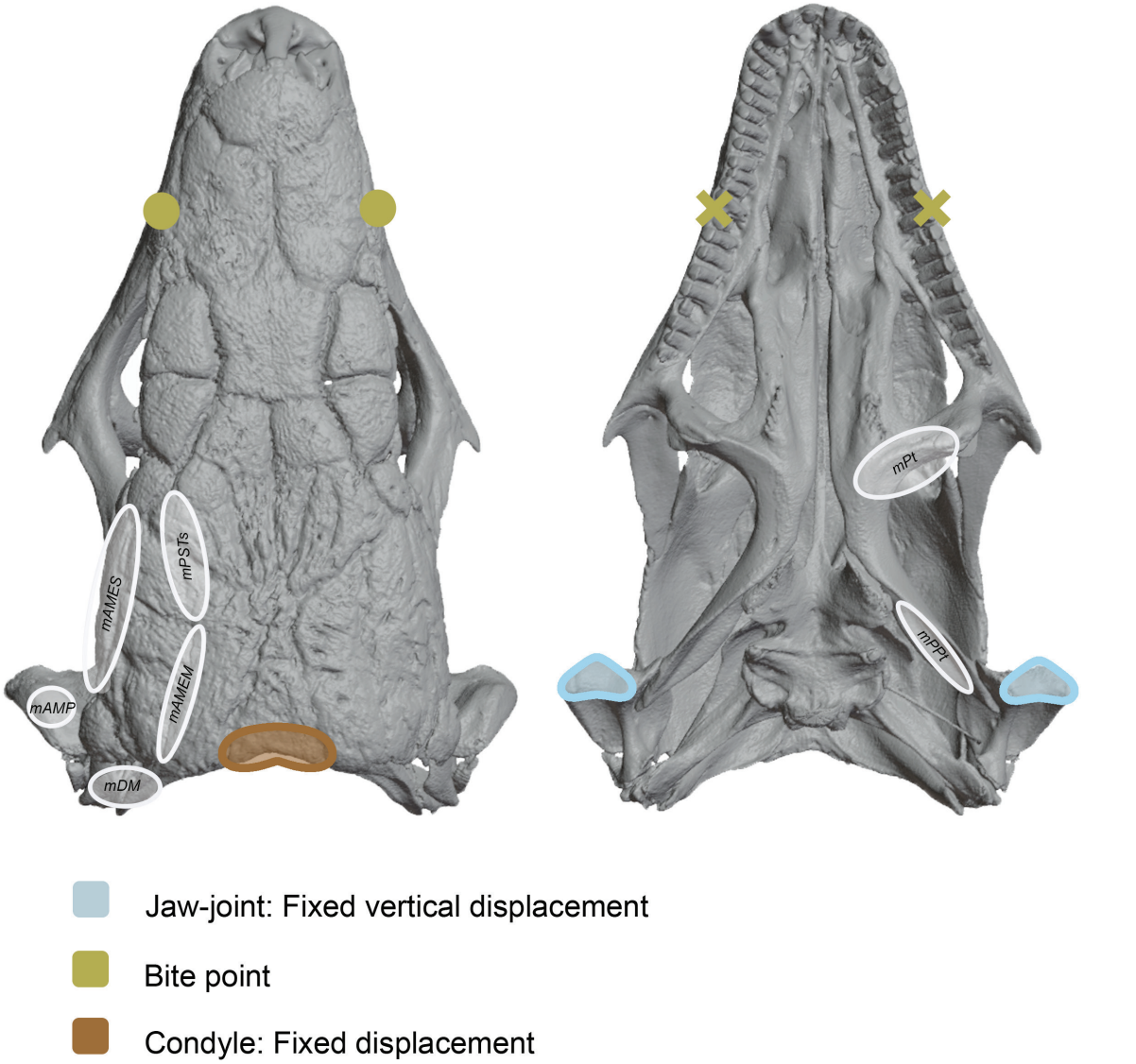

Figure 1. Boundary conditions. Selected fixation areas used across all models in finite element analysis (FEA). The condyle was constrained to prevent displacement, and a fixed vertical displacement was applied at the jaw joints to simulate articulation. The main masticatory muscles are shown, including adductor mandibulae externus superficialis (mAMES), adductor mandibulae externus medialis (mAMEM), pseudotemporalis superficialis (mPSTs), pterygoideus (mPT), depressor mandibulae (mDM), protractor pterygoideus (mPPt), and adductor mandibulae posterior (mAMP).

Anatomical abbreviations: mAMEM: m. adductor mandibulae externus medialis; mAMEP: m. adductor mandibulae externus profundus; mAMES: m. adductor mandibulae externus superficialis; mAMP: m. adductor mandibulae posterior; mDM: m. depressor mandibulae; mLPt: m. levator pterygoideus; mPPt: m. protractor pterygoideus; mPSTp: m. pseudotemporalis profundus; mPSTs: m. pseudotemporalis superficialis; mPt: m. pterygoideus.

Results

Nanoindentation analysis

Region E11 (enamel) demonstrates higher values and greater variability in comparison with other regions (Figs 2, 3; Table 4), indicating its rigidity and reduced deformability. Following E11, several bone regions, namely B7 (inner part of the dentary), B2 and B4 (central part of the parietal and central part of the pterygoid, respectively), and B3 (quadrate), generally exhibit higher *E* values than D10 (dentine), whereas B6 (coronoid) and B1 (premaxilla), along with B5 (orbital osteoderm), are among the bone regions with the lowest *E* values. In contrast, the sutural regions S8 (contact area of the frontals and parietal) and S9 (vomer–palatine suture) consistently exhibited the lowest *E* values across all specimens (Figs 2, 3, Suppl. material 9: fig. S3; Table 4), indicating that they are the most flexible cranial elements.

Despite the observed differences in stiffness values among the bone regions, the range between the largest and smallest values (13.87–28.46 GPa; Table 4) suggests moderate variability overall, which can still be considered relatively low in the context of biological tissues and thus supports the assumption of acceptable homogeneity.

At the specimen level, mean *E* values ranged from 16.88 GPa to 24.31 GPa (Table 4). The smallest specimen, with a skull length of 18.56 mm (Table 1) and identified by the label code 020322-4 (*G. atlantica*), exhibits the highest stiffness, with an *E* value of 24.31 GPa. Following an observed trend between stiffness and size, the specimen with the label code G.galloti/21-1 (*G. galloti*) ranks next, with an *E* value of 18.97 GPa. Subsequently, the adult and largest *G. stehlini*, with a skull length of 61.10 mm, has a stiffness value of 16.96 GPa, while juveniles of the same species display an average of 17.04 GPa. The smallest juvenile, *G. stehlini* (040322-3), with a skull length of 21.66 mm, is the most elastic specimen, with a value of 16.88 GPa (Table 4).

Homogeneity of Young's modulus across cranial areas (LMM 1)

The summary of the first LMM, which tested whether Young's modulus (*E*) differed among cranial areas (B1–B7) in adult *Gallotia* specimens, indicated that no individual cranial area differed significantly from the reference level (B1). The Type III ANOVA with Satterthwaite approximation confirmed that there were no significant differences in *E* among cranial areas ($F = 0.54$, p-value = 0.77). These results indicate that *E* values can be considered homogeneous across the examined cranial regions in adult specimens of *Gallotia*. A full summary and the results of LMM 1 are available in Suppl. material 7.

Relationship between Young's modulus and dorsal cranial length (LMM 2)

Results from the summary of LMM 2, which tested the relationship between Young's modulus (*E*) and dorsal cranial length (DCL) while controlling for other fixed effects ("Cranial Area" and "Ontogeny") and random effects, indicated that DCL was significantly negatively associated with *E* (DCL: $\beta = -0.12$, SE = 0.03, $t = -3.53$, p-value = 0.002). The Type III ANOVA with Satterthwaite approximation confirmed the significance of DCL ($F = 12.44$, p-value = 0.002). This finding suggests that specimens with larger crania exhibit lower *E* values than smaller specimens, supporting the use of DCL to extrapolate *E* values to extinct and closely related *Gallotia* species. LMM 2 provided both an average *E* value for the three fossil specimens (*G. goliath* DZULL 2453, *G. goliath* DZULL 2454, and *G. auaritae* PCCRULL1169) and predicted *E* values for the seven cranial bone regions of each specimen (Fig. 4). *G. goliath* DZULL 2454 had the highest predicted *E* value (16.19 GPa), whereas the other two specimens had similar, lower values (14.67 and 14.63 GPa). Predicted *E* values for each cranial bone region (B1–B7) are listed in Table 5.

The fixed effect "Cranial Area" was not significant according to the results of the Type III ANOVA ($F = 2.20$, p-value = 0.077), showing that there were no significant differences in *E* between the analysed cranial areas (B1–B7), in accordance with the previous findings from LMM 1.

As previously explained, juvenile specimens were included in LMM 2 solely to increase variation in DCL between specimens, enabling a more reliable estimation of this fixed effect, without aiming to draw strong conclusions regarding the effect of ontogeny on *E*, which could not be fully assessed due to the limited sample size and the restricted number of ontogenetic stages represented. Exploratory results indicate that the fixed effect "Ontogeny" on *E* was significant in the model ($\beta = -2.822$, SE = 1.09, $t = -2.60$, p-value = 0.015), according to the Type III ANOVA results ($F = 6.76$, p-value = 0.015), suggesting that adult individuals tend to exhibit higher *E* values than juveniles. However, a larger sample of both juvenile and adult specimens is required to draw robust conclusions regarding the effect of ontogenetic stage on *E*. The full summary and results of LMM 2 are available in Suppl. material 7.

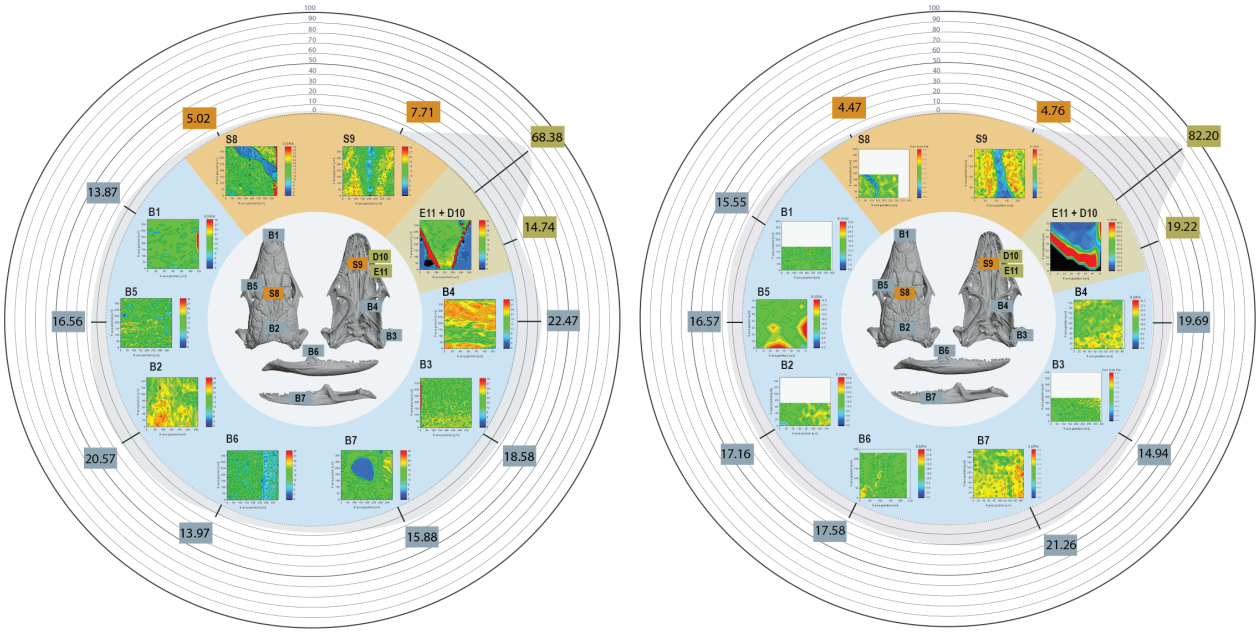

G. stehlini
Adult (GAST492-22)

G. stehlini
Juvenile (040322-1)

Figure 2. Nanoindentation results for *G. stehlini* specimens (040322_1, juvenile, left; GAST492-22, adult, right). Each circle represents the values of a specimen, with arrows indicating the corresponding anatomical zones (as defined in Table 2). The graphs display Young's modulus (GPa) in these zones, with colours representing stiffness in picometres: red for the stiffest regions and blue for the most elastic regions. White spaces mark the end of a region, varying depending on the specimen. On the outer edge of each circle, a visual representation summarises the values from Table 4, highlighting zones with higher or lower *E* values. Colours on the circle indicate the type of zone: orange for sutures (S), blue for bone (B), and green for teeth (D and E).

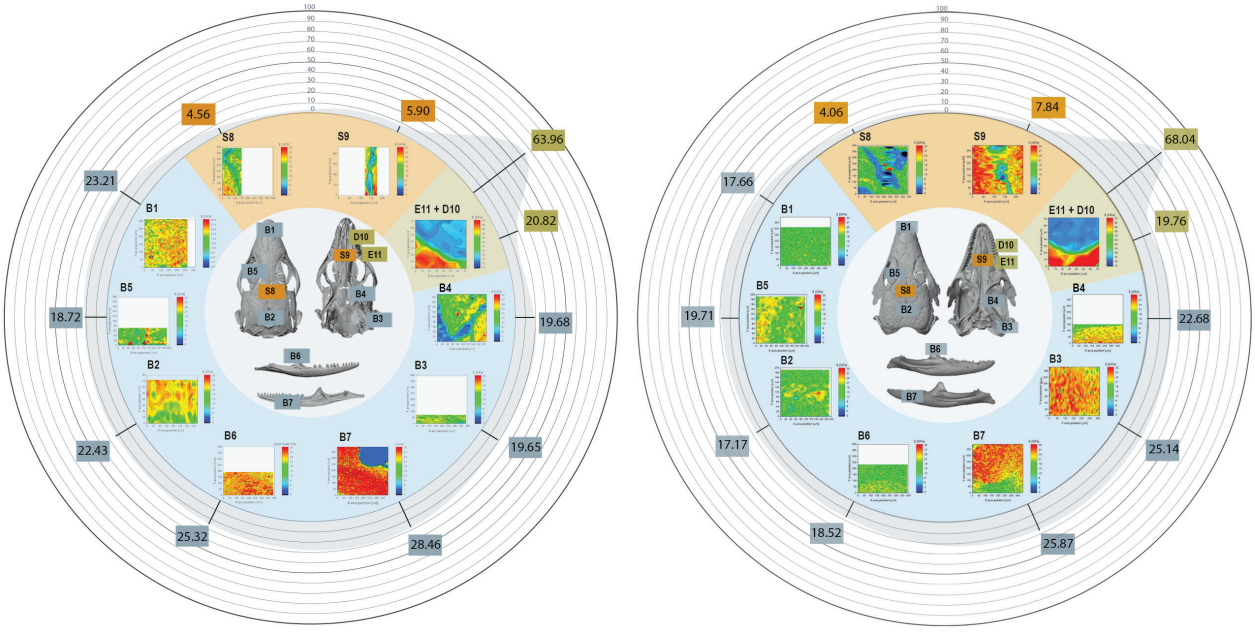

G. atlantica
(020322-4)

G. galloti
(G.galloti/21-1)

Figure 3. Nanoindentation results for *G. galloti* (G.galloti/21-1) on the left and *G. atlantica* (020322_4) on the right. Each circle represents the values of a specimen, with arrows indicating the corresponding anatomical zones (as defined in Table 2). The graphs display Young's modulus (GPa) in these zones, with colours representing stiffness in picometres: red for the stiffest regions and blue for the most elastic regions. White spaces mark the end of a region, varying by specimen. On the outer edge of each circle, a visual representation summarises the values from Table 4, highlighting zones with higher or lower *E* values. Colours on the circle indicate the type of zone: orange for sutures (S), blue for bone (B), and green for teeth (D and E).

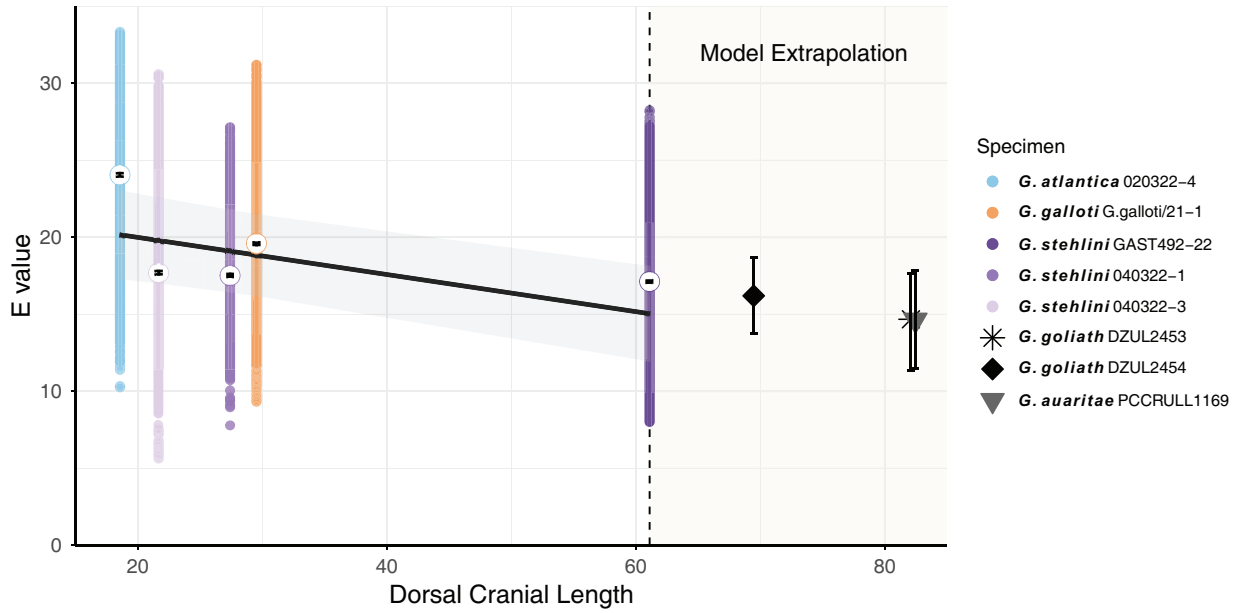

Figure 4. Relationship between dorsal cranial length (DCL; mm) and Young's modulus (*E*; GPa) in extant *Gallotia* specimens, with extrapolated mean *E* values for fossil taxa. Points represent individual measurements, and larger symbols indicate mean *E* values per specimen with 95% CIs. The solid line represents the fitted relationship from the linear mixed model (LMM 2), with the grey-shaded area indicating its 95% CI. The dashed vertical line marks the upper range of the observed DCL values in extant specimens, and values beyond this threshold represent model extrapolations (beige-shaded area).

Table 5. Bone *E* values predicted using linear mixed models for extinct specimens.

Taxon	Label	Skull length [mm]	B1	B2	B3	B4	B5	B6	B7	Predicted average E_{bone} [GPa]
G. goliath	DZULL2453	82.09	12.50	15.18	14.60	15.86	13.58	12.96	18.01	14.67
G. goliath	DZULL2454	69.46	14.03	16.70	16.12	17.38	15.11	14.48	19.54	16.19
G. auaritae	PCCRULL1169	82.45	12.46	15.13	14.56	15.81	13.54	12.92	17.98	14.63

Finite element analysis: differences between defined materials

Both heterogeneous and homogeneous material models exhibited similar patterns of stress and strain distribution, as evidenced by the von Mises stress results (Fig, 5, Suppl. material 9: fig. S4). Although slight variations in stress concentration values were observed between the two approaches, these differences were not substantial enough to indicate different mechanical behaviours based on the two materials.

Differences between species

There is a clear distinction between species when examining the von Mises stress and strain distributions, with *G. galloti* having the most resistant skull (Fig, 5, Suppl. material 9: fig. S4). *G. galloti* develops lower stress and strain values in comparison with the other species, with fewer areas of the cranium exhibiting high stress values. *G. stehlini* exhibits higher stresses and strains than *G. galloti*, specifically in the central region of the parietal and premaxilla in the dorsal part of the cranium, but it also has one of the stiffest skulls. However, *G. stehlini* experiences less stress in the pterygoid than its smaller relative, while it shows a higher range of values in the lateral regions of the parietal and neurocranium.

The fossil specimen *G. goliath* exhibits lower stress and strain in the premaxilla and anterior part of the skull, with high stress values concentrated in the vomer, palatal bones, and lateral pterygoids, distinguishing it from *G. stehlini*. In contrast to its relatives, *G. atlantica* experiences higher overall stress, particularly in the anterior and posterior skull regions, suggesting a comparatively greater susceptibility to failure under equivalent loading conditions and making it the most fragile of the species analysed.

Discussion

In this study, a distinction is made between two complementary sources of functional information derived from the skulls of *Gallotia*: (1) the intrinsic mechanical

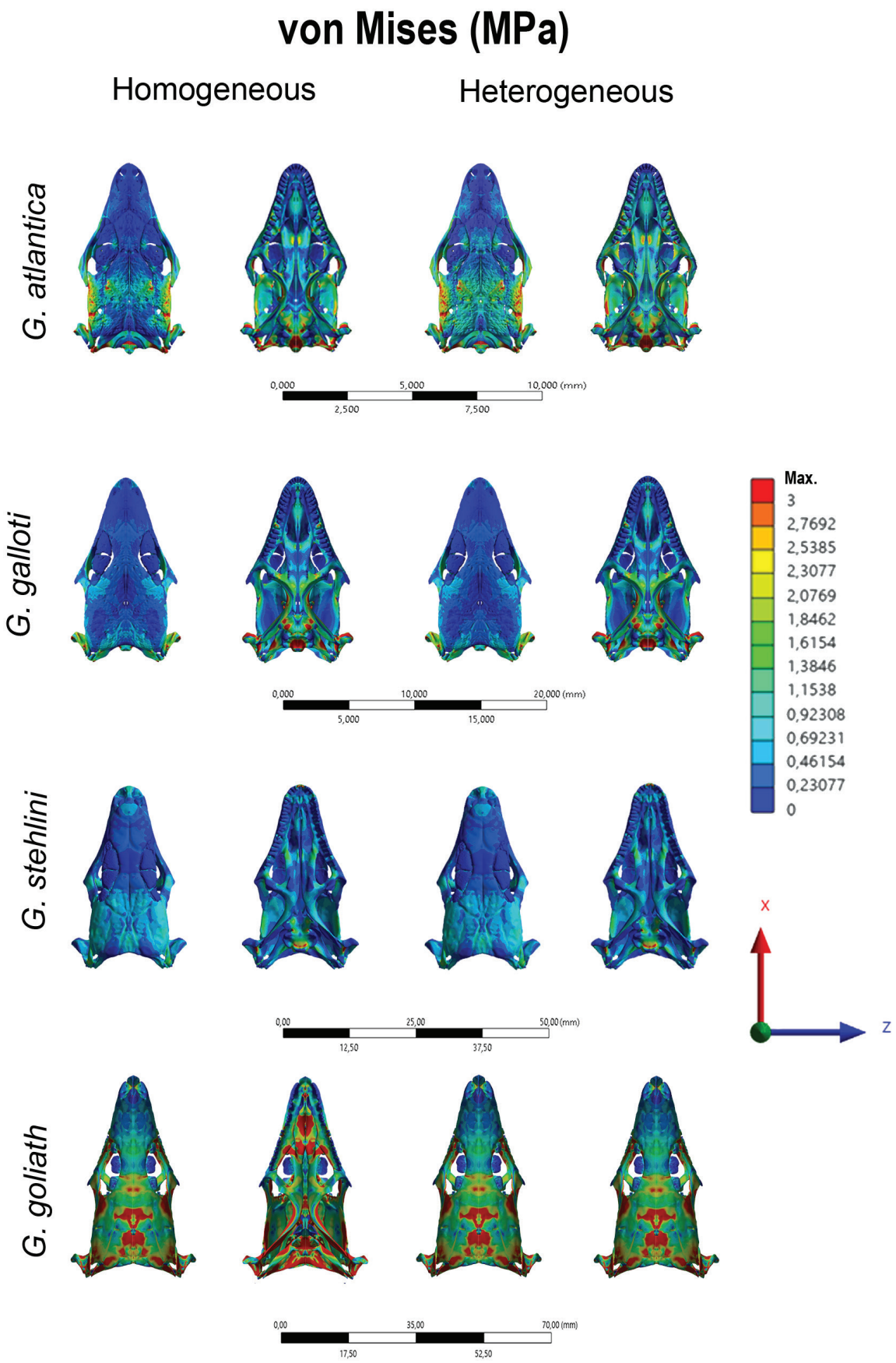

Figure 5. Von Mises stress (MPa) in the studied species: *G. atlantica*, *G. galloti*, *G. stehlini*, and *G. goliath*. Two types of models were produced: one assuming homogeneous material properties for all bones and another using specific elastic modulus values for different bone regions, derived from the nanoindentation results or inferred for *G. goliath* based on linear mixed models.

behaviour of the bone tissue, reflecting its material properties, and (2) the structural performance of the cranium as a whole, which depends on its geometry and loading conditions.

Nanoindentation analysis

Nanoindentation has proved to be an effective methodology for gathering data to test the aforementioned hypotheses regarding whether a homogeneous or heterogeneous material should be used in FEA models. Moreover, the results highlight the importance of understanding material features to assess their influence on functional morphology analyses.

The studied insular species of the genus *Gallotia* exhibited a distinct pattern indicating a negative correlation between *E* and skull size. Specifically, smaller lizards showed higher median *E* values in the bone areas (24.31 ± 4.08 GPa), while lizards with larger skulls exhibited comparatively lower median *E* values (16.96 ± 3.21 GPa). *Gallotia* taxa demonstrate distinct skull morphological variations despite close phylogenetic relationships. These variations in the correlation between skull stiffness and individual body size may be explained by the particular environmental conditions to which each species has adapted on the various islands of the archipelago (Brown et al. 2016; Molina-Borja and Bohórquez-Alonso 2023). Each island provides a unique ecological setting where species diversify to occupy vacant ecological niches, leading to morphological and functional adaptations in response to insular conditions (Benítez-López et al. 2021). This aligns with the island rule (Whittaker and Fernández-Palacios 2007), which proposes that island species often exhibit shifts in body size, with smaller species tending to become larger and larger species becoming smaller due to ecological pressures. Such conditions may include factors such as predation level, resource availability, competition level, weather fluctuations, and geological changes such as volcanism, all of which contribute to shaping the evolutionary trajectory of each species (Vitt 2000; Meiri 2008).

Diet and food resources

Results from nanoindentation analyses suggest a relationship between size and bone stiffness. This pattern may be explained by dietary differences observed among *Gallotia* species, as larger species tend to maintain a more plant-based diet throughout the year, while smaller species rely more on animal-based sources, which may be scarcer and seasonally variable. Such differences in resource availability could contribute to the observed size variation among island species, in line with general patterns of insular adaptation (e.g. Masson et al. 2023; Pinho et al. 2024). However, these results also indirectly support a relationship between size and strength. Whereas stiffness is a measure of a material's resistance to deformation, strength is its ability to withstand applied stress before failing or yielding (Cowin 2001; Currey 2006). A high *E* does not necessarily indicate a higher capacity to resist fracture or yielding. However, in cortical bone, different studies have suggested that strength is generally proportional to *E* because both properties are influenced by the bone's composition and microstructure (Doblaré et al. 2004; Currey 2006). Therefore, results from nanoindentation analysis can be interpreted as a proxy for analysing both strength and stiffness.

The stiffness of *Gallotia* skull bone is related to the dietary preferences of the species, as the different species under study also exhibit variations in their diet. In general terms, *Gallotia* taxa are classified as omnivorous (Valido and Nogales 2003), but the proportion of plant-based and animal-based food intake differs among the three analysed species. The largest species, *G. stehlini*, is mainly found on the island of Gran Canaria. Although considered omnivorous, its diet is primarily herbivorous, with a particular preference for leaves and seeds and a low intake of animal prey (Mateo and Lopez-Jurado 1992; Carretero et al. 2006). The results also display a consistent pattern that has been observed in previous studies (Hennekam et al. 2023), indicating that larger individuals tend to consume a higher proportion of plant matter. On the other hand, *G. galloti*, which has its origins on Tenerife Island but is also present on La Palma Island (Cox et al. 2010), occupies an intermediate position in terms of size when compared with its sister species. It is also classified as an omnivorous lizard, although its plant intake differs from that of *G. stehlini*, being more fruit- and nectar-based (Rodríguez et al. 2008; González-Castro and Siverio 2024). In addition to the effects of insularity, dietary habits are currently also shaped by agricultural practices on Tenerife. The availability of food resources introduced by plantations over recent centuries, such as tomatoes, strawberries, and grapes (Roca et al. 2005), provided a dietary alternative to seeds and leaves. Furthermore, the establishment of these plantations led to an overall reduction in food availability during winter, when animal-based sources became more important (Valido and Nogales 1994, 2003).

Lastly, the smallest-sized taxon, *G. atlantica* (Valido and Nogales 1994; Salvador 2015), has adapted its diet to the more arid conditions of the islands of Lanzarote and Fuerteventura. Consequently, it exhibits a higher intake of invertebrates, including hard-shelled invertebrates belonging to the orders Coleoptera, Hemiptera, and Gastropoda. Thus, this species has the least plant-based diet and consumes the toughest food items among the three studied species (Salvador 2015).

The dietary habits of vertebrates are known to directly influence cranial morphology and body size (Herrel et al. 2001; McBrayer 2004; Hennekam et al. 2023). Consequently, it is expected that a diet based on hard

food resources would require stronger bone in comparison with a soft-food diet (Marcé-Nogué et al. 2017). Thus, it is not surprising that the smallest-sized species, *G. atlantica*, with a diet based on hard-shelled invertebrates such as snails or beetles, presents the highest *E* values, followed by *G. galloti*, which has a softer diet that includes fruit but requires additional robustness to hold and crush harder invertebrates to survive through the winter, not only because of the need to crush and ingest harder structures but also because of the need to support stronger jaw muscles. Finally, the largest living species, *G. stehlini*, presents an almost vegetarian diet throughout the year and presents the lowest *E* values. Considering the relationship between *E* and bone strength described above (Doblaré et al. 2004; Currey 2006), these lower values suggest a mechanically weaker skull compared with the other analysed species, whereas higher *E* values are consistent with stronger skulls. However, this relationship should not be interpreted as a direct indicator of biting performance, as bite force depends on multiple factors, including cranial morphology, muscle architecture, and body size (Saulnier Masson et al. 2023).

Compared with continental lizards, *G. stehlini* and *G. galloti* follow an insular trend towards increased herbivory, which has morphological implications. This trend is associated with an increase in body size, as larger lizards facilitate vegetation digestion by having a longer intestinal tract that helps absorb nutrients and process tougher foods such as seeds and leaves (Schluter 1984; Zimmerman and Tracy 1989). As body and skull size increase, the need for a robust skull decreases as the strength required to process food diminishes.

In contrast, *G. atlantica*, inhabiting the islands closer to the continent, exhibits a distinct pattern. This is likely due to its initial adaptation to a new niche with limited edible vegetation and a shift towards a more insectivorous diet, with higher resource availability. This dietary shift demanded the ability to handle larger prey with minimal handling time to obtain greater energetic content (McBrayer 2004; Herrel et al. 2010).

The comparatively less robust skull and higher stress concentrations observed in *G. goliath* suggest a dietary shift towards herbivory with increased body size related to the island rule (see below), allowing effective herbivorous feeding despite a less reinforced skull.

Protection from predation

Dietary preferences are the main factors driving the mechanical behaviour of the jaw. In contrast, other factors also influence the protective role of the brain and sensory structures (Tseng and Flynn 2018). Therefore, the material properties obtained from nanoindentation suggest a trend more strongly associated with size and diet, although other functional influences cannot be ruled out.

Smaller species, such as *G. atlantica*, face higher predation pressure from a greater variety of predators. Not only is *G. atlantica* preyed upon by common predators shared with *G. stehlini* and *G. galloti* – such as common ravens or cats – but its smaller body size also makes it more vulnerable to smaller predators. These include small mammals such as hedgehogs and shrews, as well as smaller bird species such as shrikes or Berthelot's pipit (Valido and Nogales 1994, 2003). Smaller species of this genus are also found on islands closer to the continent, where they face more predators and competitors due to easier island colonisation through time. The higher immigration rate of species from the mainland further intensifies these pressures.

The increased predation risk faced by smaller lizards might further contribute to the evolution of a stronger cranium by enhancing the protection of vital areas where predation pressure is high. In contrast, the results obtained for the extinct giant species *G. goliath* are possibly a consequence of the island rule (Palkovacs 2003; McNab 2010): these animals had very high resource availability and low or no predation and competition levels before humans settled on these islands (Castillo et al. 1994). The latter was possibly related only to birds, without the presence of cats, humans, or snakes, as occurs today.

In this regard, results from the nanoindentation tests would indicate that *G. atlantica* has the stiffest skull among the four species studied. However, the conclusion that *G. atlantica* has the stiffest skull does not necessarily imply that it is the most resistant overall, as the material properties of the skull were the sole parameters analysed, while geometry plays a crucial role in the overall mechanical resistance of the cranium and the distribution of stress, making a skull more or less resistant to failure. Accordingly, FEA reveals that, under identical biting conditions, *G. galloti* exhibits lower stress values than the other analysed species. Within the context of the simulated feeding scenario, this suggests a greater capacity to withstand biting-related loads without approaching structural limits. Although the models were not designed to evaluate resistance to predatory compression directly, this mechanical behaviour may also reflect comparatively greater overall cranial robustness.

This is not what would be expected if dietary preferences were the only factor shaping skull design, as *G. galloti* is not the species with the highest proportion of hard food in its diet. Therefore, it is suggested that protection against predation may have been an additional factor influencing the morphology of *G. galloti*, resulting in a comparatively more robust skull, with bony structures that may be more resistant to potential fractures. This may contribute to explaining why this species is widespread across different islands and occupies a broader range of ecological niches. In contrast, *G. atlantica* exhibits overall higher stress and strain values under the tested loading conditions, suggesting lower structural resistance than the other taxa. This may have implications beyond feeding performance, indicating that its evolutionary history has been shaped by multiple interacting factors, as previously discussed.

From a methodological perspective, the comparisons between homogeneous and heterogeneous material assignments showed very similar patterns of stress and strain distribution. Given that no significant differences in *E* were found among the cranial areas analysed, the homogeneous approach appears to be the most appropriate for the present case.

Conclusion

The application of nanoindentation analysis to the study of the biomechanical behaviour of the lizard genus *Gallotia* during biting has significantly advanced understanding of skull biomechanics, particularly in relation to Young's modulus and its spatial variation across cranial regions. The results indicate that *E* values do not differ significantly among the analysed bone areas, supporting the use of an average *E* value to represent the mechanical behaviour of the skull in this genus. This finding simplifies the parameterisation of future biomechanical models without compromising their biological accuracy and highlights *Gallotia* as a valuable system for studying cranial functional trade-offs. The effects of the absence of the lower temporal bar are a prime example of this, as all analysed species share this feature but exhibit species-specific tension patterns in the jugal, quadrate, and postorbital, likely reflecting adaptations unique to each species and its particular ecological niche.

By integrating FEA with nanoindentation data, a more comprehensive understanding of skull resistance in the genus *Gallotia* was achieved. FEA highlights the role of cranial morphology in modulating mechanical performance – either amplifying or mitigating stress levels – beyond what material properties alone can explain. In this case, the findings show that morphological adaptations among insular species arise in response to environmental pressures. Differences in skull resistance reflect distinct evolutionary strategies shaped by factors such as prey availability, predation risk, and environmental challenges, including anthropogenic impacts.

In particular, *G. stehlini* and *G. goliath* display morphological and ecological traits consistent with the island rule, whereby herbivory in insular environments favours increased body size to enhance digestive efficiency. In general terms, the results closely align with field observations, validating the combined use of nanoindentation and FEA as a reliable framework for investigating mechanical properties.

When evaluating the two tested hypotheses, (A) that spatial heterogeneity in bone stiffness is required for biologically realistic FEA results and (B) that a homogeneous Young's modulus is sufficient to capture global skull mechanical behaviour, hypothesis (B) is therefore supported. The results show that when Young's modulus is assumed to be homogeneous and incorporated into the model using the mean value across all bone regions, outcomes do not differ significantly from those obtained with a heterogeneous approach. This suggests that, at the scale of the mechanical responses examined here, averaged material properties are sufficient to capture the global biomechanical performance of the skull. However, heterogeneous models remain advantageous when local stress or strain distributions are of interest or when taxa show strong structural differentiation. Therefore, the choice between homogeneous and heterogeneous approaches should depend on the biological question and the required level of spatial resolution.

Future research should broaden the scope of specimens studied – including sex information, ontogenetic stages, and individuals with diverse diets and environmental adaptations – to better understand how these factors shape skull morphology and robustness. In addition, integrating new modelling approaches, such as the inclusion of kinesis or sutures (Garcia-Escolà et al. 2024), into FEA would provide deeper insights into how bone density and microstructure affect mechanical performance. Comparative studies across different island ecosystems would help determine whether similar adaptive patterns occur in other insular species.

Acknowledgements

The authors thank Yael Hernandez Santana, Jose Manuel Caballero Fernández, and Mario Jesus Navarro Aponte for collecting the *G. atlantica*, *G. galloti*, and young *G. stehlini* specimens analysed by nanoindentation. The participation of Yael Hernández Santana was supported by the XI Convocatoria del Programa de Mecenazgo Alumni – Universidad de La Laguna. The authors thank the Canary Government for the legal permits required to analyse *Gallotia* specimens. We thank Francesco Della Giustina, an anonymous reviewer, and the editor for their constructive comments and suggestions, which helped improve the manuscript. The authors also acknowledge the helpful comments by Thomas Püschel on the statistical analysis. This article is part of the PhD dissertation of L.G.E. within the framework of the PhD Programme in Biodiversity of the Universitat Autònoma de Barcelona.

References

Aguirre TG, Ingrole A, Fuller L, Seek TW, Fiorillo AR, Sertich JJW, Donahue SW (2020) Differing trabecular bone architecture in dinosaurs and mammals contributes to stiffness and limits on bone strain. PLOS ONE 15: e0237042. https://doi.org/10.1371/journal.pone.0237042

Alexander RM (1992) Exploring Biomechanics: Animals in Motion. Scientific American Library.

Allison PG, Rodriguez RI, Moser RD, Williams BA, Poda AR, Seiter JM, Lafferty BJ, Kennedy AJ, Chandler MQ (2014) Characterization of multi-layered fish scales (*Atractosteus spatula*) using nanoin-

dentation, X-ray CT, FTIR, and SEM. J Vis Exp 89: e51535. https://doi.org/10.3791/51535

Barahona F, Barbadillo LJ, Sánchez-Herráiz MJ (1998) Osteological variation in *Lacerta lepida* (Reptilia: Lacertidae) and its implications for cranial kinesis. Journal of Morphology 236: 1–8.

Barel CDN (1983) Towards a constructional morphology of cichlid fishes (Teleostei, Perciformes). Netherlands Journal of Zoology 33: 357–424. https://doi.org/10.1163/002829683x00183

Bates D, Mächler M, Bolker B, Walker S (2015) Fitting linear mixed-effects models using lme4. Journal of Statistical Software 67: 1–48. https://doi.org/10.18637/jss.v067.i01

Benítez-López A, Santini L, Gallego-Zamorano J, Milá B, Walkden P, Huijbregts MAJ, Tobias JA (2021) The island rule explains consistent patterns of body size evolution in terrestrial vertebrates. Nature Ecology & Evolution 5: 768–786. https://doi.org/10.1038/s41559-021-01426-y

Brown CM, Vavrek MJ (2015) Small sample sizes in the study of ontogenetic allometry: Implications for palaeobiology. PeerJ 3: e818. https://doi.org/10.7717/peerj.818

Brown RP, Paterson S, Risse J (2016) Genomic signatures of historical allopatry and ecological divergence in an island lizard. Genome Biology and Evolution 8: 3618–3626. https://doi.org/10.1093/gbe/evw268

Button DJ, Rayfield EJ, Barrett PM (2014) Cranial biomechanics underpins high sauropod diversity in resource partitioning. Proceedings of the Royal Society B: Biological Sciences 281: 20142114. https://doi.org/10.5061/dryad.8kd16

Carretero M, Roca V, Martín J, Llorente G, Montori A, Santos X, Mateos J (2006) Diet and helminth parasites in the Gran Canaria giant lizard, *Gallotia stehlini*. Revista Española de Herpetología 20: 105–117.

Castillo C, Rando JC, Zamora JF (1994) Discovery of mummified extinct giant lizards (*Gallotia goliath*, Lacertidae) in Tenerife, Canary Islands. Bonner Zoologische Beiträge 45: 129–136. https://doi.org/10.5281/zenodo.13445498

Core Team (2018) R: A Language and Environment for Statistical Computing. https://doi.org/10.32614/r.manuals

Cox SC, Carranza S, Brown RP (2010) Divergence times and colonization of the Canary Islands by Gallotia lizards. Molecular Phylogenetics and Evolution 56: 747–757. https://doi.org/10.1016/j.ympev.2010.03.020

Cowin SC (2001) Bone mechanics handbook (2nd ed.). CRC Press. https://doi.org/10.1115/1.1579463

Cruzado-Caballero P, Castillo Ruiz C, Bolet A, Colmenero JR, De la Nuez J, Casillas R, Llacer S, Bernardini F, Fortuny J (2019) First nearly complete skull of *Gallotia auaritae* (lower-middle Pleistocene, Squamata, Gallotiinae) and a morphological phylogenetic analysis of the genus *Gallotia*. Scientific Reports 9: 16629. https://doi.org/10.1038/s41598-019-52244-z

Cuff AR, Bright JA, Rayfield EJ (2015) Validation experiments on finite element models of an ostrich (*Struthio camelus*) cranium. PeerJ 3: e1294. https://doi.org/10.7717/peerj.1294

Cuff AR, Rayfield EJ (2013) Feeding Mechanics in Spinosaurid Theropods and Extant Crocodilians. PLOS ONE 8(5): e65295. https://doi.org/10.1371/journal.pone.0065295

Currey JD (1987) The evolution of the mechanical properties of amniote bone. Journal of Biomechanics 20: 1035–1044. https://doi.org/10.1016/0021-9290(87)90021-2

Currey JD (2006) Bones: Structure and Mechanics. Princeton University Press.

Cuy JL, Mann AB, Livi KJ, Teaford MF, Weihs TP (2002) Nanoindentation mapping of the mechanical properties of human molar tooth enamel. Archives of Oral Biology 47: 281–291. https://doi.org/10.1016/S0003-9969(02)00006-7

Della Giustina F, Gaudichon VF, Boman R, Chatar N, MacLaren JA, Fischer V (2026) Distinct feeding biomechanics in Late Cretaceous marine reptiles from the Western Interior Seaway. Palaeontology 69: e70051. https://doi.org/10.1111/pala.70051

Doblaré M, García JM, Gómez MJ (2004) Modelling bone tissue fracture and healing: a review. Engineering Fracture Mechanics 71: 1809–1840. https://doi.org/10.1016/j.engfracmech.2003.08.003

Dutel H, Gröning F, Sharp AC, Watson PJ, Herrel A, Ross CF, Jones MEH, Evans SE, Fagan MJ (2021) Comparative cranial biomechanics in two lizard species: impact of variation in cranial design. The Journal of Experimental Biology 224: jeb234831. https://doi.org/10.1242/jeb.234831

Erickson GM, Catanese J, Keaveny TM (2002) Evolution of the biomechanical material properties of the femur. The Anatomical Record 268: 115–124. https://doi.org/10.1002/ar.10145

Evans SE (2008) The skull of lizards and tuatara. In Biology of the Reptilia 20: 1–347.

Garcia-Escolà L, Fortuny J, Marcé-Nogué J (2024) A new biomechanical approach to cranial suture function: the role of contact elements in linear and nonlinear models. Paleobiology 50: 503–511. https://doi.org/10.1017/pab.2024.19

Gómez-Benito MJ, García-Aznar JM, Doblaré M (2005) Finite element prediction of proximal femoral fracture patterns under different loads. Journal of Biomechanical Engineering 127: 9–14. https://doi.org/10.1115/1.1835347

González-Castro A, Siverio F (2024) Flower-visiting lizards as key ecological actors for an endemic and critically endangered plant in the Canary Islands. Journal of Pollination Ecology 36: 88–103. https://doi.org/10.26786/1920-7603(2024)777

Hennekam JJ, Herridge VL, Cox PG (2023) Feeding biomechanics reveals niche differentiation related to insular gigantism. Evolution 77: 1303–1314. https://doi.org/10.1093/evolut/qpad041

Herrel A, De Vree F, Delheusy V (1999) The mechanical basis of biting performance and feeding behaviour in lizards. Journal of Experimental Biology 202: 3519–3530. https://doi.org/10.1242/jeb.202.24.3687

Herrel A, De Grauw E, Lemos-Espinal JA (2001) Head shape and bite performance in xenosaurid lizards. Journal of Experimental Zoology 290: 101–107. https://doi.org/10.1002/jez.1039

Herrel A, Vanhooydonck B, Van Damme R (2001) Evolution of bite performance in lizards: adaptive patterns in relation to diet. Functional Ecology 15: 289–295.

Herrel A, Moore JA, Bredeweg EM, Nelson NJ (2010) Sexual dimorphism, body size, bite force and male mating success in tuatara. Biological Journal of the Linnean Society 100: 287–292. https://doi.org/10.1111/j.1095-8312.2010.01433.x

Herrel A, Schaerlaeken V, Meyers JJ, Metzger KA, Ross CF (2014) The evolution of cranial design and performance in squamates: consequences of skull-bone reduction on feeding behaviour. Anatomical Record 297: 1113–1125.

Hoaglin DC, Iglewicz B, Tukey JW (1986) Performance of some resistant rules for outlier labeling. Journal of the American Statistical Association 81: 991–999. https://doi.org/10.1080/01621459.1986.10478363

Iordansky NN (2010) Cranial kinesis in lizards (Reptilia: Squamata): origin, biomechanics, and evolution. Biology Bulletin 37: 868–877. https://doi.org/10.1134/S1062359011090032

Jones MEH, Gröning F, Dutel H, Sharp A, Fagan MJ, Evans SE (2017) The biomechanical role of the chondrocranium and sutures in a lizard cranium. Journal of The Royal Society Interface 14: 20170637. https://doi.org/10.1098/rsif.2017.0637

Keyak JH, Rossi SA, Jones KA, Skinner HB (1998) Prediction of femoral fracture load using automated finite element modeling. Journal of Biomechanics 31: 125–133. https://doi.org/10.1016/S0021-9290(97)00123-1

Klingenberg CP (1998) Heterochrony and allometry: the analysis of evolutionary change in ontogeny. Biological Reviews 73(1): 79–123. https://doi.org/10.1017/S000632319800512X

Krings W, Marcé-Nogué J, Gorb SN (2021) Finite element analysis relating shape, material properties, and dimensions of taenioglossan radular teeth with trophic specialisations in Paludomidae (Gastropoda). Scientific Reports 11: 2102. https://doi.org/10.1038/s41598-021-02102-8

Kuznetsova A, Brockhoff PB, Christensen RHB (2017) lmerTest package: tests in linear mixed effects models. Journal of Statistical Software 82: 1–26. https://doi.org/10.18637/jss.v082.i13

Lautenschlager S, Ferreira GS, Werneburg I (2018) Sensory evolution and ecology of early turtles revealed by digital endocranial reconstructions. Frontiers in Ecology and Evolution 6: 7. https://doi.org/10.3389/fevo.2018.00007

Lüdecke D (2018) ggeffects: tidy data frames of marginal effects from regression models. Journal of Open Source Software 3: 772. https://doi.org/10.21105/joss.00772

Lüdecke D, Ben-Shachar MS, Patil I, Waggoner P, Makowski D (2021) performance: an R package for assessment, comparison and testing of statistical models. Journal of Open Source Software 6: 3139. https://doi.org/10.21105/joss.03139

Marcé-Nogué J, Fortuny J, Gil L, Galobart À (2011) Using reverse engineering to reconstruct tetrapod skulls and analyse its feeding behaviour. Proceedings of the 13th International Conference on Civil, Structural and Environmental Engineering Computing: 237. https://doi.org/10.4203/ccp.96.237

Marcé-Nogué J, Püschel TA, Kaiser TM (2017) A biomechanical approach to understand the ecomorphological relationship between primate mandibles and diet. Scientific Reports 7: 8364. https://doi.org/10.1038/s41598-017-08161-0

Marghoub A, Williams CJA, Leite JV, Kirby AC, Kéver L, Porro LB, Barrett PM, Bertazzo S, Abzhanov A, Vickaryous M, Herrel A, Evans SE, Moazen M (2022) Unravelling the structural variation of lizard osteoderms. Acta Biomaterialia 146: 306–316. https://doi.org/10.1016/j.actbio.2022.05.004

Mateo JA, Lopez-Jurado LF (1992) Study of dentition in lizards from Gran Canaria Island (Canary Islands) and its ecological and evolutionary significance. Biological Journal of the Linnean Society 46: 39–48. https://doi.org/10.1111/j.1095-8312.1992.tb00848.x

Mateo JA, Geniez P, Veiret P, López-Jurado LF (2022) Reptiles de la Macaronesia: Azores, Madeira, Salvajes, Canarias, Cabo Verde y litoral del Sáhara atlántico. Asociación Herpetológica Española.

Mazzetta GV, Cisilino AP, Blanco RE, Calvo N (2009) The mechanical design of the skull of Tyrannosaurus rex: insights from a finite element analysis. Anatomical Record 292: 426–439. https://doi.org/10.1671/039.029.0313

McBrayer LD (2004) The relationship between skull morphology, biting performance and foraging mode in Kalahari lacertid lizards. Zoological Journal of the Linnean Society 140: 403–416. https://doi.org/10.1111/j.1096-3642.2003.00106.x

McGuire JA, Dudley R (2011) The biology of gliding in flying lizards (Genus *Draco*) and their fossil and extant analogs. Integrative and Comparative Biology 51(6): 983–990. https://doi.org/10.1093/icb/icr090

McNab BK (2010) Geographic and temporal correlations of mammalian size reconsidered: a resource rule. Oecologia 164: 13–23. https://doi.org/10.1007/s00442-010-1621-5

Meiri S (2008) Evolution and ecology of lizard body sizes. Global Ecology and Biogeography 17: 724–734. https://doi.org/10.1111/j.1466-8238.2008.00414.x

Mezzalira SM (2013) Phylogenetic analysis of cranial kinesis evolution in Squamata. Zoological Journal of the Linnean Society 169: 711–725.

Mitchell D, Wroe S, Martin M, Weisbecker V (2025) Testing hypotheses of skull function with comparative finite element analysis: three methods reveal contrasting results. The Journal of Experimental Biology 228: jeb249747. https://doi.org/10.1242/jeb.249747

Moazen M, Curtis N, Evans SE, O'Higgins P, Fagan MJ (2008) Combined finite element and multibody dynamics analysis of biting in a Uromastyx hardwickii lizard skull. Journal of Anatomy 213: 499–508. https://doi.org/10.1111/j.1469-7580.2008.00980.x

Molina-Borja M, Bohórquez-Alonso ML (2023) Morphology, behaviour and evolution of *Gallotia* lizards from the Canary Islands. Animals 13: 2319. https://doi.org/10.3390/ani13142319

Montuelle SJ, Williams SH (2015) In vivo measurement of mesokinesis in *Gekko gecko*: The role of cranial kinesis during gape display, feeding and biting. PLOS ONE 10: e0134710. https://doi.org/10.1371/journal.pone.0134710

Oliver WC, Pharr GM (1992) An improved technique for determining hardness and elastic modulus using load and displacement sensing indentation experiments. Journal of Materials Research 7: 1564–1583. https://doi.org/10.1557/JMR.1992.1564

Oliver WC, Pharr GM (2004) Measurement of hardness and elastic modulus by instrumented indentation: advances in understanding and refinements to methodology. Journal of Materials Research 19: 3–20. https://doi.org/10.1557/jmr.2004.19.1.3

Palacios-García S, Cruzado-Caballero P, Casillas R, Ruiz CC (2021) Quaternary biodiversity of the giant fossil endemic lizards from the island of El Hierro (Canary Islands, Spain). Quaternary Science Reviews 262: 106961. https://doi.org/10.1016/j.quascirev.2021.106961

Palkovacs EP (2003) Explaining adaptive shifts in body size on islands: a life history approach. Oikos 103: 37–44. https://doi.org/10.1034/j.1600-0706.2003.12502.x

Paluh DJ, Bauer AM (2018) Phylogenetic history, allometry and disparate functional pressures influence the morphological diversification of the gekkotan quadrate, a keystone cranial element. Biological Journal of the Linnean Society 125: 693–708. https://doi.org/10.1093/biolinnean/bly147

Pérez-Martín S, Fortuny J, Cruzado-Caballero P, Bernardini F, Castillo Ruiz C (2023) In the jaws of a titan: 3D comparative anatomy of the mandibles of the Canary giant lizards (Gallotiinae: Gallotia). Historical Biology 35: 1052–1068. https://doi.org/10.1080/08912963.2022.2077107

Pinho CJ, Dinis HA, Emerson BC, Vasconcelos R (2024) Smaller islands, bigger appetites: evolutionary strategies of insular endem-

ic skinks. Royal Society Open Science 11: 240870. https://doi.org/10.1098/rsos.240870

Pinho CJ, Dinis HA, Emerson BC, Vasconcelos R (2024) Smaller islands, bigger appetites: evolutionary strategies of insular endemic skinks. Royal Society Open Science 11: 240870. https://doi.org/10.1098/rsos.240870

Rayfield E (2007) Finite element analysis and understanding the biomechanics and evolution of living and fossil organisms. Annual Review of Earth and Planetary Sciences 35: 541–576. https://doi.org/10.1146/annurev.earth.35.031306.140104

Revelle W (2025) psych: Procedures for psychological, psychometric, and personality research. R package. https://doi.org/10.32614/cran.package.psych

Roca V, Carretero MA, Llorente GA, Montori A, Martin JE (2005) Helminth communities of two lizard populations (Lacertidae) from Canary Islands (Spain): host diet-parasite relationships. Amphibia-Reptilia 26: 535–542. https://doi.org/10.1163/156853805774806160

Rodríguez A, Nogales M, Rumeu B, Rodríguez B (2008) Temporal and spatial variation in the diet of the endemic lizard *Gallotia galloti* in an insular Mediterranean scrubland. Journal of Herpetology 42: 213–222. https://doi.org/10.1670/07-0752.1

Rodríguez-Florez N, Oyen ML, Shefelbine SJ (2013) Insight into differences in nanoindentation properties of bone. Journal of the Mechanical Behavior of Biomedical Materials 18: 90–99. https://doi.org/10.1016/j.jmbbm.2012.11.005

Salvador A (2015) Lagarto gigante de Gran Canaria – *Gallotia stehlini*. In Enciclopedia Virtual de los Vertebrados Españoles. http://www.vertebradosibericos.org

Saulnier Masson R, Daoues K, Measey J, Herrel A (2023) The evolution of bite force and head morphology in scincid lizards: diet and habitat use as possible drivers. Biological Journal of the Linnean Society 140: 58–73. https://doi.org/10.1093/biolinnean/blad052

Schluter D (1984) A variance test for detecting species associations, with some example applications. Ecology 65: 998–1005. https://doi.org/10.2307/1938071

Tseng ZJ, Flynn JJ (2018) Structure-function covariation with nonfeeding ecological variables influences evolution of feeding specialization in Carnivora. Science Adventure 4: eaao5441. https://doi.org/10.1126/sciadv.aao5441

Tukey JW (1977) Exploratory data analysis. Addison-Wesley Publishing Company.

Valido A, Nogales M (1994) Frugivory and seed dispersal by the lizard Gallotia galloti (Lacertidae) in a xeric habitat of the Canary Islands. Oikos 70: 403–411. https://doi.org/10.2307/3545778

Valido A, Nogales M (2003) Digestive ecology of two omnivorous Canarian lizard species (Gallotia, Lacertidae). Amphibia-Reptilia 24: 331–344. https://doi.org/10.1163/156853803322440790

Villa A, Delfino M (2019) A comparative atlas of the skull osteology of European lizards (Reptilia: Squamata). Zoological Journal of the Linnean Society 187: 829–928. https://doi.org/10.1093/zoolinnean/zlz035

Vitt LJ (2000) Ecological consequences of body size in neonatal and small-bodied lizards in the Neotropics. Herpetological Monographs 14: 388–400. https://doi.org/10.2307/1467053

Wang L, Meloro C, Fagan MJ, Kissane RWP, Bates KT, Askew GN, Watson PJ (2024) Regional variation of the cortical and trabecular bone material properties in the rabbit skull. PLOS ONE 19: e0298621. https://doi.org/10.1371/journal.pone.0298621

Westneat MW (2003) A biomechanical model for analysis of muscle force, power output and lower jaw motion in fishes. Journal of Theoretical Biology 223: 269–281. https://doi.org/10.1016/S0022-5193(03)00058-4

Whittaker RJ, Fernández-Palacios JM (2007) Island Biogeography: Ecology, Evolution, and Conservation. Oxford University Press. https://doi.org/10.1093/oso/9780198566113.001.0001

Wickham H (2016) ggplot2: Elegant graphics for data analysis. Springer-Verlag. https://ggplot2.tidyverse.org

Witmer LM (1995) The extant phylogenetic bracket and the importance of reconstructing soft tissues in fossils. In Functional Morphology in Vertebrate Paleontology: 19–33.

Zimmerman LC, Tracy CR (1989) Interactions between the environment and ectothermy and herbivory in reptiles. Physiological Zoology 62: 374–409. https://doi.org/10.1086/physzool.62.2.30156176

Additional information

Conflict of interest

The authors have declared that no competing interests exist.

Ethical statement

No ethical statement was reported.

Artificial Intelligence (AI) use

The authors accept full responsibility for the content of the manuscript, including the disclosure of any use of AI.
No AI tools were used in the preparation of this manuscript.

Funding

This research was funded by the Agencia Estatal de Investigación (AEI) of the Spanish Ministerio de Ciencia e Innovación through the R+D+I projects PID2020-117118GB-I00/AEI/10.13039/501100011033 and PID2024-156593NB-I00, co-funded by MICIU/AEI/10.13039/501100011033 and the European Union (FEDER, UE). Research has also been supported by the Generalitat de Catalunya/CERCA Programme; the Agència de Gestió d'Ajuts Universitaris i de Recerca of the Generalitat de Catalunya (2021 SGR 01184 to JF and SGR2021-01239 to JMN); a Juan de la Cierva contract (JDC2023-050836-I) to AdC, financed by the Agencia Estatal de Investigación of the Ministerio de Ciencia e Innovación of Spain (MCIN/AEI/10.13039/501100011033); and a 'Ramón y Cajal' contract RYC2021-032857-I to J.F., financed by the Agencia Estatal de Investigación of the Ministerio de Ciencia e Innovación of Spain (MCIN/AEI/10.13039/501100011033), the European Union "NextGenerationEU"/PRTR, and the Ministerio de Ciencia e Innovación together with the European Regional Development Fund (AEI/FEDER, EU) under project PID2021-122612OB-I00. JMN acknowledges support from the Universitat Rovira i Virgili (2023PFR-URV-1239). Finally, this work also benefited from the financial support of the projects PROID1017010136, funded by the Canary Islands Government, and 2017REC20, funded by Fundación CajaCanarias.

Author contributions

Laia Garcia-Escolà: Writing – original draft, Investigation, Methodology, Formal analysis, Conceptualization. Jordi Marcé-Nogué: Conceptualization, Methodology, Investigation, Formal analysis, Writing – review and editing. Ane de Celis: Data curation, Methodology, Formal analysis, Writing. Nuria Cuadrado: Methodology, Formal analysis. Eduard Vidales: Methodology, Formal analysis. Penélope Cruzado-Caballero: Resources, Writing – review and editing. Alejandro Serrano-Martínez: Data curation, Methodology, Formal analysis, Writing – review and editing. Carolina Castillo-Ruiz: Resources, Writing – review and editing. Josep Fortuny: Conceptualization, Investigation, Writing – review and editing, Data curation, Project administration, Funding acquisition.

Author ORCIDs

L. Garcia-Escolà https://orcid.org/0009-0006-2818-734X
J. Marcé-Nogué https://orcid.org/0000-0001-9852-7027
A. de Celis https://orcid.org/0000-0002-7362-7360
N. Cuadrado https://orcid.org/0000-0002-3745-2372
E. Vidales https://orcid.org/0000-0002-4346-3481
P. Cruzado-Caballero https://orcid.org/0000-0002-5819-8254
A. Serrano-Martínez https://orcid.org/0000-0003-1178-6064
C. Castillo-Ruiz https://orcid.org/0000-0003-3381-7490
J. Fortuny https://orcid.org/0000-0003-4282-1619

Data availability

The raw CT data and derived 3D models are available through the MorphoSource repository https://www.morphosource.org/projects/000716569.

Supplementary material 1

Summary of the number of indentations and sample size for each zone across five individuals: *G_Stehlini-040322_3*, *G_Stehlini-040322_1*, *G_Sthelini-492-22*, *G_Atlantica-020322_4*, and *G_Galloti 121-1*

Authors: Laia Garcia-Escolà, Jordi Marcé-Nogué, Ane de Celis, Nuria Cuadrado, Eduard Vidales, Penélope Cruzado-Caballero, Alejandro Serrano-Martínez, Carolina Castillo-Ruiz, Josep Fortuny

Data type: ods

Link: https://doi.org/10.3897/sjp.145.193019.suppl1

Supplementary material 2

Results from the nanoindentation arrays on the areas of interest in the cranium and mandible of *G. atlantica* 020322-4

Authors: Laia Garcia-Escolà, Jordi Marcé-Nogué, Ane de Celis, Nuria Cuadrado, Eduard Vidales, Penélope Cruzado-Caballero, Alejandro Serrano-Martínez, Carolina Castillo-Ruiz, Josep Fortuny

Data type: ods

Explanation note: The dataset comprises a total of 6450 measurements across the entire skull and have been filtered to remove outliers and values not representative of the analysed tissue.

Link: https://doi.org/10.3897/sjp.145.193019.suppl2

Supplementary material 3

Results from the nanoindentation arrays on the areas of interest in the cranium and mandible of *G. stehlini* 040322-3

Authors: Laia Garcia-Escolà, Jordi Marcé-Nogué, Ane de Celis, Nuria Cuadrado, Eduard Vidales, Penélope Cruzado-Caballero, Alejandro Serrano-Martínez, Carolina Castillo-Ruiz, Josep Fortuny

Data type: ods

Explanation note: The dataset comprises a total of 8436 measurements across the entire skull and have been filtered to remove outliers and values not representative of the analysed tissue.

Link: https://doi.org/10.3897/sjp.145.193019.suppl3

Supplementary material 4

Results from the nanoindentation arrays on the areas of interest in the cranium and mandible of *G. stehlini* GAST492-22

Authors: Laia Garcia-Escolà, Jordi Marcé-Nogué, Ane de Celis, Nuria Cuadrado, Eduard Vidales, Penélope Cruzado-Caballero, Alejandro Serrano-Martínez, Carolina Castillo-Ruiz, Josep Fortuny

Data type: ods

Explanation note: The dataset comprises a total of 13285 measurements across the entire skull and have been filtered to remove outliers and values not representative of the analysed tissue.

Link: https://doi.org/10.3897/sjp.145.193019.suppl4

Supplementary material 5

Results from the nanoindentation arrays on the areas of interest in the cranium and mandible of *G. stehlini* (040322-1)

Authors: Laia Garcia-Escolà, Jordi Marcé-Nogué, Ane de Celis, Nuria Cuadrado, Eduard Vidales, Penélope Cruzado-Caballero, Alejandro Serrano-Martínez, Carolina Castillo-Ruiz, Josep Fortuny

Data type: ods

Explanation note: The dataset comprises a total of 4714 measurements across the entire skull and have been filtered to remove outliers and values not representative of the analysed tissue.

Link: https://doi.org/10.3897/sjp.145.193019.suppl5

Supplementary material 6

Results from the nanoindentation arrays on the areas of interest in the cranium and mandible of *G. stehlini* (040322-3)

Authors: Laia Garcia-Escolà, Jordi Marcé-Nogué, Ane de Celis, Nuria Cuadrado, Eduard Vidales, Penélope Cruzado-Caballero, Alejandro Serrano-Martínez, Carolina Castillo-Ruiz, Josep Fortuny

Data type: ods

Explanation note: The dataset comprises a total of 6398 measurements across the entire skull and have been filtered to remove outliers and values not representative of the analysed tissue.

Link: https://doi.org/10.3897/sjp.145.193019.suppl6

Supplementary material 7

Results of all statistical tests performed with the complete dataset comprising 39,284 measurements per area across all species

Authors: Laia Garcia-Escolà, Jordi Marcé-Nogué, Ane de Celis, Nuria Cuadrado, Eduard Vidales, Penélope Cruzado-Caballero, Alejandro Serrano-Martínez, Carolina Castillo-Ruiz, Josep Fortuny
Data type: ods
Explanation note: The file includes descriptive statistics, outputs of the two principal linear mixed models, and fossil prediction calculations.

Link: https://doi.org/10.3897/sjp.145.193019.suppl7

Supplementary material 8

Scripts for the statistical analysis of data in R, including those used for the two linear mixed models (LMM1 and LMM2) and for the descriptive statistics applied in the methodology

Authors: Laia Garcia-Escolà, Jordi Marcé-Nogué, Ane de Celis, Nuria Cuadrado, Eduard Vidales, Penélope Cruzado-Caballero, Alejandro Serrano-Martínez, Carolina Castillo-Ruiz, Josep Fortuny
Data type: R File

Link: https://doi.org/10.3897/sjp.145.193019.suppl8

Supplementary material 9

Supplementary text, figures and tables

Authors: Laia Garcia-Escolà, Jordi Marcé-Nogué, Ane de Celis, Nuria Cuadrado, Eduard Vidales, Penélope Cruzado-Caballero, Alejandro Serrano-Martínez, Carolina Castillo-Ruiz, Josep Fortuny
Data type: docx

Link: https://doi.org/10.3897/sjp.145.193019.suppl9